Applied Physics A manuscript No.
(will be inserted by the editor)

Terahertz wave emission from plasmonic chiral metasurfaces

Takahiro Matsui · Satoshi Tomita · Motoki Asai · Yuzuru Tadokoro · Keisuke Takano · Makoto Nakajima · Masanori Hangyo · Hisao Yanagi

Received: date / Accepted: date

Abstract Plasmonic chiral metasurfaces with pinwheel-like structures are fabricated on silver films using a focused ion-beam milling technique. In time-domain spectroscopy, we observe terahertz (THz) wave emission from metasurfaces irradiated by a near-infrared Ti:Sapphire ultra-short pulsed laser. The origin of the THz wave generation is likely to be tunnelling ionization accompanied with photoelectron acceleration by ponderomotive force. Numerical simulation is carried out toward improvement of the chiral metasurfaces for better emission of circularly polarized THz waves.

Keywords Metasurfaces · Terahertz waves · Chirality · Optical activity

1 Introduction

As a new class of metamaterials, two dimensional microstructures called metasurfaces are of great interest [1,2]. It is known that plasmonic nanoparticle arrays, which are similar to metasurfaces, emit terahertz (THz) waves by irradiation of a pulsed laser [3–5]. This is a promising technique for new functional THz wave sources. Metasurfaces with the broken space-inversion symmetry (that is, chirality) may emit circularly polarized THz waves, which can be utilized for a novel THz scanner [6]. However, because chirality requires three dimensional (3D) structures, how chirality is incorporated into metasurfaces remains a challenge. Standard micro-processing with photolithography and etching is applicable in the preparation of planar chirality [7], but not with 3D chiral structures. Contrastingly, a focused ion-beam (FIB) milling technique would be advantageous toward the realization of metasurfaces including 3D structures.

T. Matsui, S. Tomita, H. Yanagi
Graduate School of Materials Science, Nara Institute of Science and Technology, Ikoma, Nara 630-0192, Japan
Tel.: +81-743-72-6015
E-mail: tomita@ms.naist.jp

M. Asai, Y. Tadokoro, K. Takano, M. Nakajima, M. Hangyo
Institute of Laser Engineering, Osaka University, Suita, Osaka 565-0871, Japan

In this paper, we prepare silver (Ag) films with pinwheel-like structures – plasmonic chiral metasurfaces– using a FIB milling technique. THz time-domain spectroscopy (THz-TDS) demonstrates that THz waves are emitted from the metasurfaces irradiated by ultra-short pulse laser. The mechanism of the THz wave emission is discussed. Moreover, numerical simulation suggests how chiral metasurfaces can be improved for emission of circularly polarized THz waves.

2 Sample Fabrication and THz Time-Domain Spectroscopy

Ag films 300 nm in thickness were deposited on fused quartz substrates by magnetron sputtering. Chiral metasurfaces were prepared on the Ag films using the FIB (FB-2200AN, Hitachi) milling technique. The metasurfaces consisted of pinwheel-like structures with rectangular pits 1.2 μm in length and 0.3 μm in width. One pinwheel structure comprised four rectangles. In the rectangles, staircase-like slopes were fabricated consisting of ten 30 nm-height-steps. The down-stair direction defined the "pinwheel direction". We prepared the metasurfaces with pinwheel-like structures in both clock-wise (CW) and counter-clock-wise (CCW) directions. Three hundred pinwheels were fabricated in a 60 μm $\times$ 40 μm area.

The generation and detection of THz wave were carried out using amplified Ti:Sapphire ultra-short pulse laser (Mai Tai and Spitfire, Spectra-Physics) in standard THz-TDS [3, 4, 8]. The center wavelength, pulse width, and repetition rate of the laser were 800 nm, 35 fsec, and 1 kHz, respectively. The pulsed laser beam was split into two beams: one illuminating the metasurfaces for the generation of the THz pulses, the other going to a ZnTe 110-oriented electro-optical (EO) crystal used for the detection of the emitted THz pulses. The excitation beam diameter illuminating the metasurfaces was 2.2 mm as evaluated using the knife method. The maximum intensity of the excitation beam was approximately 80 GW/cm^2 and the intensity was varied using a neutral density filter. The incident angle of the excitation beam was 45 degree with p-polarization.

Emitted THz waves were collected by parabolic mirrors and focused onto the EO crystal for detection. Since the THz pulses were much longer than the Ti:Sapphire ultra-short pulses, the electric field of the emitted THz wave was regarded as a static electric field biasing detection EO crystal. The THz field thus induced birefringence in the crystal, modifying the polarization state of the 800 nm detection beam coincident with the THz pulse on the crystal. The change in polarization state was measured using a polarizing beam splitter and a pair of balanced photodiodes. A quarter waveplate before the beam splitter was used to ensure that the polarization states were balanced when no THz field was emitted. By varying the delay between THz and probe pulses the temporal profile of the THz field was obtained. Moreover, rotation angle and ellipticity of the THz waves were analyzed with two wire-grid polarizers between the sample and detector.

3 Experimental Results

Figure 1 shows a scanning electron microscopic (SEM) image of the CCW chiral metasurfaces of Ag. Array of pinwheel-like structures is observed in Fig. 1(a).

Figure 1(b) is an enlarged image of the pinwheel-like structure. The size of rectangular pits in the pinwheel was 1.2 μm in length and 0.3 μm in width, which were very similar to those designed in the FIB fabrication. Arrows indicate the down-stair direction. It is seen that we have succeeded in fabricating staircase-like slopes in the pits with the CCW pinwheel. Pinwheel-like structures in the CW chiral metasurfaces were very similar to those observed in Fig. 1(a) while the down-stair direction was opposite to that in Fig. 1(a).

Figure 2 shows electric field amplitude of emitted THz waves as a function of delay time. Red circles and blue squares correspond to signals from the CW and CCW chiral metasurfaces, respectively. CW and CCW chiral metasurfaces show peaks in the amplitude at approximately 5 psec, which is arbitrary determined by the position of the delay stage. No THz emission was observed from Ag film without pinwheel-like pits (black crosses). Frequency domain spectra obtained by the Fourier transformation of the time-domain signals are shown in the inset. THz emission is seen in frequencies between 0.2 to 1.5 THz with a peak at approximately 0.5 THz. These results demonstrate that the plasmonic chiral metasurfaces emit THz waves.

In Fig. 3, the intensity of the THz waves emitted from the CW (red circles) and CCW (blue squares) chiral metasurfaces are plotted as a function of incident laser power between 20 and 80 GW/cm^2. Note that the THz intensity corresponds to the square of the electric field amplitude of the emitted THz waves. Broken lines are fitted lines. The numbers in the bracket are the fitted orders of the lines associated with the data. Figure 3 shows that the order parameters of the generation of the THz radiation from both chiral metasurfaces are close to two.

Rotation angle and ellipticity of the emitted THz waves were analyzed with two wire-grid polarizers between the sample and detector in the THz-TDS. However, rotation angle and ellipticity were very small and the emitted THz pulse was almost a *p*-polarized wave. In the following, we carried out numerical calculation to find the improved chiral metasurfaces for emission of circularly polarized THz waves.

4 Numerical Simulation Results

Full-wave electromagnetic field calculation was carried out using the finite element method (ANSYS HFSS). Figure 4(a) illustrates a bird's-eye view of the unit cell of the improved chiral metasurface in numerical calculation. The metasurface consists of four rectangular pits with slopes as shown in Fig. 4(a). The calculated metasurface is similar to that shown in Fig. 1 although the size of the rectangular pits is smaller in the calculation (rectangular pits 100 nm in width, 700 nm in length, and 0 to 200 nm in depth). Nevertheless, the metasurfaces can be prepared using the FIB milling technique.

The greatest difference between our calculation and experiment is the altitude of the starting point of the slopes. By calculation, the starting point of the rectangular pits are lowered gradually in the pinwheel-like structures. Figure 4(b) depicts a cross-sectional view of the developed unit cell. An orange circle with an arrow indicates the starting point of the first slope in Fig. 4(b) and Fig. 4(a). The first slope goes down 200 nm in depth. While slope depths are identically 200 nm, the

starting points of the second, third, and fourth slopes are lowered d_z, $2d_z$ and $3d_z$, respectively, from the initial starting point, as shown in Fig. 4(b).

Figures 4(c)-4(f) show calculated reflection spectra (left) and electric field distributions at specific frequencies (right) with $d_z = 0$ nm, 40 nm, 80 nm, and 120 nm. The incident and reflection angles of light are normal to the surface. Solid lines in the reflection spectra correspond to simulation with Ag, whereas dashed lines correspond to gold (Au). The calculated result indicates that a change in metal from Ag to Au does not affect the reflection spectra. Therefore the following discussion focuses on the simulation with Ag because experiments were carried out using Ag chiral metasurfaces.

The left-hand side of Fig. 4(c) shows reflection spectra of the chiral metasurface with $d_z = 0$ nm, similar to the metasurface studied in the experiments. The red and blue lines correspond to R_{xx} and R_{yx}. R_{xx} (R_{yx}) is assigned to reflection of the wave with the electric field in the x (y) direction when metasurfaces were irradiated by the wave with the electric field in the x direction. In other words, R_{yx} represents an optical activity of the metasurfaces.

R_{xx} in Fig. 4(c) shows a dip at 314 THz while R_{yx} shows no peak at the frequency. As shown in the right-hand side of Fig. 4(c), electric field distribution at 314 THz is symmetric. The resonance at 314 THz corresponding to the wavelength of approximately 890 nm in vacuum, is attributed to the symmetric mode at the metasurfaces. The simulation shows that the metasurface with $d_z = 0$ nm, similar to those experimentally studied, has resonance but does not show the optical activity with the 800 nm Ti:Sapphire pulse for excitation.

What we found in the numerical calculation was emergence of the optical activity with a symmetry breaking in the z direction; that is, as d_z increases, peaks in R_{yx} emerge. The left-hand side of Fig. 4(d) shows reflection spectra of the chiral metasurface with $d_z = 40$ nm. R_{xx} shows a sharp dip at 210 THz and at this frequency R_{yx} shows a peak. This is a manifestation of the optical activity by the metasurface. Indeed electric field distribution at 210 THz in the right-hand side of Fig. 4(d) is asymmetric. Moreover, the field distribution indicates the first-order mode.

As d_z is increased to 80 nm [Fig. 4(e)], the peak in R_{yx} is enhanced and shifted to a lower frequency at 176 THz. Another peak in R_{yx} emerges at 212 THz. The right hand side of Fig. 4(e) corresponds to the electric field distribution at 212 THz. The field distribution shows that the peak at this frequency is caused by the second-order mode. The peaks due to the first- and second-order asymmetric modes shift to lower frequencies at 148 THz and 194 THz when d_z is further increased to 120 nm [Fig. 4(f)]. The field distribution at 148 THz clearly shows that the asymmetric first-order mode. These numerical results indicate that chiral metasurfaces with lowered starting points in the rectangular pits show resonant optical activities with the excitation beam.

5 Discussion

Figure 3 shows order parameters for the generation of THz radiation from the chiral metasurfaces close to two. This result suggests the second order nonlinear processes, such as optical rectification, as a possible origin for the THz generation in the metasurfaces [4]. However, Polyushkin and co-workers [8] revealed that the

optical rectification mainly contributes to the THz generation at a low incident intensity below 10 GW/cm^2. Alternatively, the order parameters close to two suggest that tunnelling ionization followed by acceleration of photogenerated electrons by ponderomotive force is likely an origin of the THz generation at a high intensity above 10 GW/cm^2 [3]. The acceleration is caused by spacial inhomogeneities in the local electric fields, resulting in ponderomotive action. The THz pulses are finally generated due to time-varying photocurrents. Further studies at a lower pump power are necessary to completely disclose the emission mechanism in the chiral metasurfaces.

Resonant excitation of the plasmonic modes on the metasurfaces is a powerful technique for emitting THz wave at a much lower pump power. In particular, as we discussed above, the resonant optical activity accompanied with spatially asymmetric electric field distributions for generating asymmetric photocurrent is critically important for emission of the circularly polarized THz waves. As shown in Fig. 4(d)-4(f), the peaks in R_{yx} are a sign of resonant optical activities with spatially asymmetric modes. Numerical results suggest that a larger d_z results in more significant symmetry breaking in the z -direction, leading to strong asymmetric distributions of electric fields at the chiral metasurfaces. The asymmetric field distribution causes asymmetric photocurrent, bringing about emission of circularly polarized THz waves.

Chiral metasurfaces with $d_z = 80$ nm are in principle viable using the FIB milling technique. Moreover, resonant excitation of the asymmetric mode at 212 THz (1.4 μm in wavelength) is plausible by optical parametric amplifier (OPA). The present study predicts that when the asymmetric modes are resonantly excited using infrared OPA, the chiral metasurfaces with $d_z = 80$ nm emit circularly polarized THz wave.

6 Conclusions

We prepared plasmonic chiral metasurfaces with pinwheel-like structures on Ag films using the FIB milling technique. We observed THz wave emission from the metasurfaces irradiated by a near-infrared Ti:Sapphire ultra-short pulsed laser in the standard THz-TDS. Tunnelling ionization followed by acceleration of photogenerated electrons by ponderomotive force was likely the origin of the THz wave generation. Numerical simulation suggested how chiral metasurfaces can be improved for emission of circularly polarized THz waves. We found that chiral metasurfaces with lowered starting points in the rectangular pits show much stronger optical activity with the excitation beam, indicating a candidate for new functional sources of circularly polarized THz waves.

Acknowledgements The authors acknowledge valuable contribution by K. Miyake in the FIB milling and fruitful discussion with K. Iwami and S. Ohno. English proofreading by L. McDowell is also acknowledged. This work was supported by MEXT/JSPS KAKENHI (Grants No. 22109003, No. 22109005, and No. 26287065).

References

1. N. Yu et al., "Light Propagation with Phase Discontinuities: Generalized Laws of Reflection and Refraction," Science, Vol. 334, 333-337, 2011.
2. N. Yu et al., "A Broadband, Background-Free Quarter-Wave Plate Based on Plasmonic Metasurfaces," Nano Letters, Vol. 12, 6328-6333, 2012.
3. D. K. Polyushkin et al., "THz Generation from Plasmonic Nanoparticle Arrays," Nano Letters, Vol. 11, 4718-4724, 2011.
4. G. Ramakrishnan and P. C. M. Planken, "Percolation-enhanced generation of terahertz pulses by optical rectification on ultrathin gold films," Optics Letters, Vol. 36, 2572-2574, 2011.
5. L. Luo et al., "Broadband terahertz generation from metamaterials," Nature Communications, 5:3055, 2014.
6. H. Suo et al., "Polarization property of terahertz wave emission from gammadion-type photoconductive antennas," Applied Physics Letters, Vol. 103, 111106, 2013.
7. K. Konishi et al., "Circularly Polarized Light Emission from Semiconductor Planar Chiral Nanostructures," Physical Review Letters, Vol. 106, 057402, 2011.
8. D. K. Polyushkin et al., "Mechanisms of THz generation from silver nanoparticle and nanohole arrays illuminated by 100 fs pulses of infrared light," Physical Review B, Vol. 89, 125426, 2014.

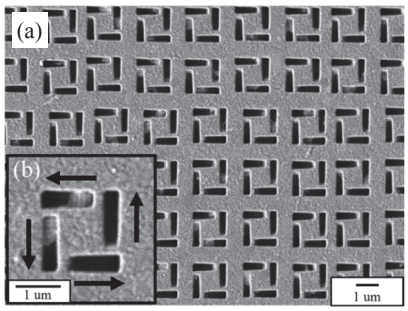

Fig. 1 (a) SEM image of CCW chiral metasurface on Ag film. (b) Enlarged image of a pinwheel-like structure. Arrows indicate the down-stair direction.

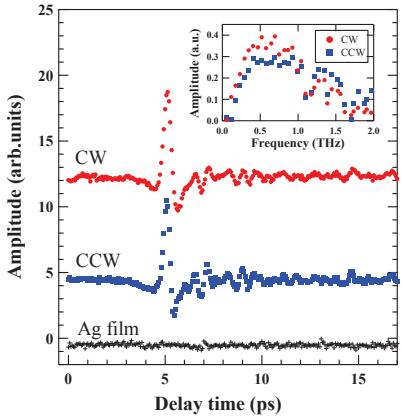

Fig. 2 Electric field amplitude of emitted THz waves observed in THz-TDS of CW (red circles) and CCW (blue squares) chiral metasurfaces. Signal from Ag film without pinwheel-like structures is also shown as black crosses. Inset: Frequency domain spectra of emitted THz waves derived by the Fourier transformation of the THz-TDS signals.

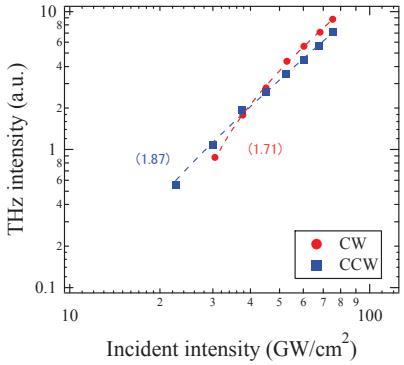

Fig. 3 THz wave intensity emitted from the CW (red circles) and CCW (blue squares) chiral metasurfaces as a function of pump power. Broken lines are fitted lines. The numbers in the bracket are the fitted orders of the lines associated with the data.

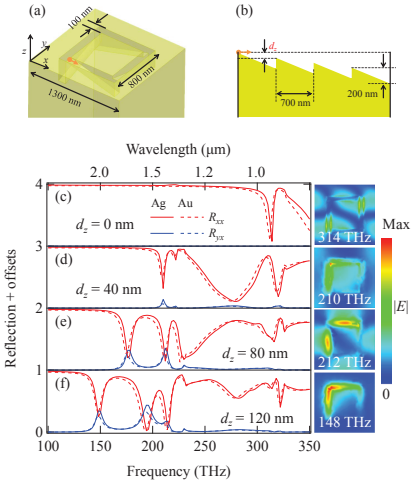

Fig. 4 (a) Bird's-eye view of the unit cell of the improved chiral metasurface for numerical calculation and (b) cross-sectional view of the developed unit cell. (c)-(f) simulated reflection spectra and electric field distribution with $d_z = 0$ nm, 40 nm, 80 nm, and 120 nm. Red and blue lines correspond to R_{xx} and R_{yx}, respectively. Solid and dashed lines correspond to simulation results with Ag and Au, respectively.